RSC Advances

PAPER

View Article Online
View Journal | View Issue

Cite this: RSC Adv., 2014, 4, 35215

Electrochemical properties of an $AgInS_2$ photoanode prepared using ultrasonic-assisted chemical bath deposition

Fang-Yun Lee,[a] Kai-Yu Yang,[a] Yi-Chen Wang,[a] Chien-Hung Li,[b] T. Randall Lee[b] and Tai-Chou Lee*[a]

Received 27th February 2014
Accepted 29th July 2014

DOI: 10.1039/c4ra01728e

www.rsc.org/advances

This study focuses on preparing a $AgInS_2$ film electrode and studying its electrochemical properties. The $AgInS_2$ film after 400 °C thermal treatment had the orthorhombic structure and a direct energy band gap of 1.98 eV. The thickness of $AgInS_2$ film used in this study was 758.9 ± 40.9 nm. In order to understand the photoelectrochemical properties, electrochemical impedances of the $AgInS_2$ photoanode in response to a light intensity of 75 mW cm^{-2} were scrutinized. It was found that homogeneous $AgInS_2$ films were obtained with increasing coatings. In addition, these dense films can effectively suppress the dark current. Charge transfer resistance and space charge capacitance can be retrieved from impedance spectra by fitting the experimental data to the models. In fact, Randle's model fitted the data better than other complicated models. Under illumination, the space charge capacitance and charge transfer resistance are strongly correlated to the onset of the photo-enhanced current density, suggesting a direct carrier transfer to the electrolyte from the valence band of the semiconductor photoanode, rather than from the surface states.

Introduction

Ternary I–III–VI_2 compounds are direct energy-gap semiconductors, and find a wide variety of applications in light emitting diodes, nonlinear optics, and photovoltaic solar cells.[1,2] For example, $CuInS_2$ and $Cu(Ga:In)Se_2$ are thin film solar cell materials with demonstrated efficiencies of 12.5% and 18.8%, respectively.[3,4] The $AgInS_2$ is a I–III–VI_2 semiconductor with a band gap energy between 1.8 and 2.0 eV. It has a tetragonal chalcopyrite (ch-$AgInS_2$) structure at low temperatures and an orthorhombic (o-$AgInS_2$) structure at higher temperatures.[5] $AgInS_2$ is considered to be a good solar cell absorber and a promising candidate to make efficient $CdS/AgInS_2/CuInSe_2$ tandem solar cells.[6–8] In addition, the electrical and optical properties of $AgInS_2$ are dominated by donor-like defects. As a consequence, it usually exhibits n-type conductivity.[1]

Recently, these ternary metal sulfide thin films, $AgInS_2$ and $AgIn_5S_8$, were used as the photoelectrode for the oxidation process.[9–12] The reported photocurrent density was relatively high, on the order of a few mA cm^{-2}, depending on the preparation method, crystal structure, and applied bias. However, the detailed mechanism for the charge transfer process of this material is missing. Additionally, the anodic reaction was usually carried out in Na_2S and K_2SO_3 sacrificial reagent due to inevitable photocorrosion. As a consequence, a relatively stable and uniform thin film electrode is required for mechanistic charge transfer investigations under illumination. Among various preparation methods, ultrasonic-assisted chemical bath deposition (UCBD) seems to be a reasonable choice. It is a simple and cost-efficient chemical process.[13,14] The reaction takes place in the dissolved precursors generally in aqueous solution at low temperatures (30–80 °C). Our previous study showed that the photoelectrode prepared using UCBD remained intact after the course of a 10 h reaction in the sacrificial reagents, with only a 10% drop in photocurrent density.[15] The 10 h time frame should be long enough for complete mechanistic studies under illumination.

Here, electrochemical impedance spectroscopy (EIS) was used to study the charge transfer pathways in the dark and under illumination. It has been reported in the literature that useful information can be extracted from the impedance measurement by interpretation of the data with suitable physical models.[16–20] In general, for the n-type semiconductor electrode, two charge transfer routes can be assumed (here only simplified models are presented): one from valence band (Fig. 1a) and the other from surface state (Fig. 1b).[20] The recombination centers, given by $R_{trapping}$, trap electrons from the conduction band and holes from the valence band. If the charge transfer follows the valence band mechanism, direct charge transfer of holes to the donor species in solution is

[a]Department of Chemical and Materials Engineering, National Central University, 300 Jhongda Rd. Jhongli, Taoyuan 320, Taiwan. E-mail: taichoulee@ncu.edu.tw
[b]Department of Chemistry and the Texas Center for Superconductivity, University of Houston, 4800 Calhoun Road, Houston, Texas 77204, USA

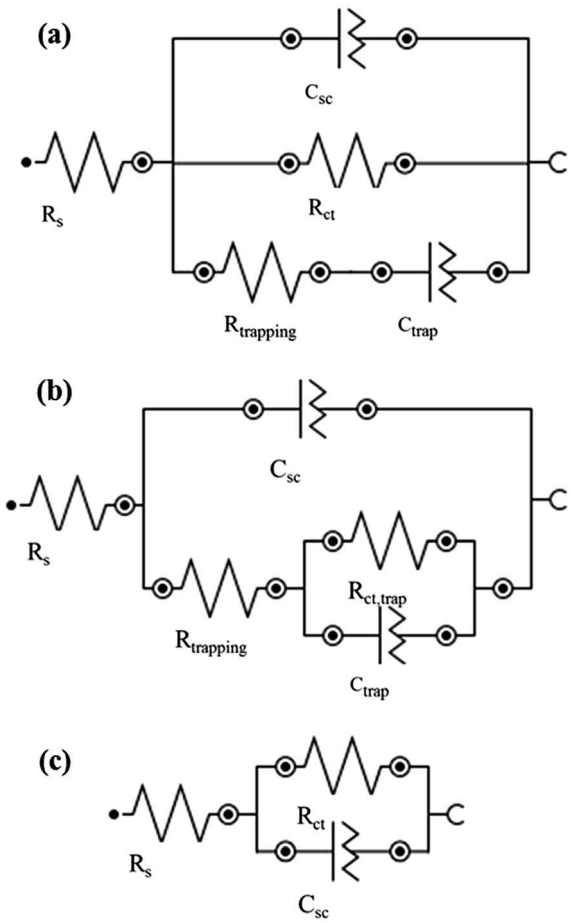

Fig. 1 Equivalent circuits for the charge carrier dynamics in photoanodes. The models corresponding to (a) charge transfer dominated from the valence band, taking into account the surface states; (b) charge transfer from the surface states, (c) Randle's model.

denoted as R_{ct} (Fig. 1a), whereas the surface states can also affect the charge transfer resistance, denoted by $R_{ct,trap}$ (Fig. 1b). If one cannot distinguish the two capacitances, space charge capacitance (C_{sc}) and charge transfer capacitance (C_{trap}), Randle's model is usually adopted (Fig. 1c).

In this study, firstly we reported the deposition of $AgInS_2$ thin films on ITO-coated glass substrates using the UCBD process. Results showed that thin films with the orthorhombic structure were obtained. Secondly, the EIS measurements were carried out in the dark and under illumination with various light intensities. In order to eliminate the photocorrosion that might interfere with the interpretation of the data, a lower light intensity of 75 mW cm^{-2} was used. It was found that, one semicircle was observed for EIS measurements both in the dark and under illumination at all applied potentials, see the detailed discussion in the following paragraph. The data suggests that the valence band charge transfer was the decisive pathway for the $AgInS_2$ film electrode. This finding can support the high photocurrent density of Ag–In–S semiconductor materials, resulting from the efficient charge transfer of holes to the sacrificial reagents.

Experimental details

Preparation of $AgInS_2$ photoelectrode

All the chemicals in the study were used as received, without any purification process. The Ag–In–S semiconductor thin films were deposited on the indium tin oxide (ITO)-coated glass substrates using ultrasonic-assisted chemical bath deposition. The substrates were first cut into slides in the size of 1 cm × 5 cm. They were then cleaned subsequently in ethanol, deionized (DI) water, and acetone, respectively in an ultrasonic bath for 30 minutes. Finally, the substrates were rinsed thoroughly with DI water and then dried with ultra-pure nitrogen gas.

Precursor solutions were prepared separately into two bottles. Solution A provides the metal ions, consisting of a mixture of 5 mL of 0.4 M silver nitrate ($AgNO_3$, 99%, Mallinckrodt), 5 mL of 0.08 M indium nitrate ($In(NO_3)_3 \cdot H_2O$, 99%, Alfa Aesar), 2.5 mL of 0.4 M ammonium nitrate (NH_4NO_3, 98%, Riedel-de Haen), and 2.5 mL of 7.4 M triethanolamine ($N(CH_2CH_2OH)_3$, 99%, Sigma Aldrich). Pure sulfuric acid (95–97%, Merck) was used to adjust the pH value of the aqueous solution to around 0.5. In this Ag/In ratio, the amount of H_2SO_4 was 10 mL. Solution A was stirred for 90 min before use. Solution B contained sulfur source, which was 0.4 M thioacetamide (CH_3CSNH_2, 99%, Merck).

The detailed experimental procedure was reported elsewhere.[11,21–23] A brief description is given here. 15.6 mL of solution B poured into 4.4 mL of solution A in a thermostat bath set at 80 °C. The substrates were then vertically immersed into the precursor solution in an ultrasonic bath. The precursor solution was used immediately after preparation. The substrates were dipped for 60 min for each deposition. After the reaction, the as-deposited thin films were thoroughly washed with DI-water in an ultrasonic bath for 5 min and then dried at 100 °C for 10 min to remove the loosely absorbed particles. The films were annealed in vacuum at 400 °C for 1 h. The deposition process can be repeated for several times for desired thickness. Finally, the samples were then cut in halves to make each of the photoelectrode with active area of 1 cm × 1 cm. According to our previous report, the silver to indium ratio was kept at 5 to prepare $AgInS_2$ thin films. Note that the Ag/In ratio of the prepared film is different from that in the precursor solution. The detailed study can be found in the literature.[22]

Materials characterizations

The morphologies of the samples and surface structures were studied using a field-emission scanning electron microscope (FEI Nova Nano SEM 230). The thicknesses of the films were determined by cross-section SEM images. The thickness of ITO was subtracted. Energy-dispersive X-ray spectrometer (EDS) attached to FE-SEM was employed to analyze the composition of the thin films. The crystal structures of the samples were determined using Bruker D2 Phaser X-ray diffractometer. The XRD patterns were recorded in the 2θ range from 20° to 70° and at the scan rate of 2° min^{-1}. The optical properties of the films were measured using a UV-vis spectrometer (Varian Cary 100), in the wavelength range of 400 to 800 nm at room temperature.

This UV-visible spectrometer is equipped with an integrating sphere. The transmission and reflection spectra were obtained by using an identical ITO-coated glass substrate as the reference. The optical energy band gaps of the films were determined by the absorption edges. The Raman vibrational spectra were obtained using a Thermo Fisher DXR Raman Microscope. The vibration peaks were indexed with the data reported in the literature.

Photoelectrochemical (PEC) and electrochemical impedance spectroscopy (EIS) measurements

Photoelectrochemical measurements were carried out using a standard three-electrode system, including a semiconductor thin film as the working electrode, a Pt plate electrode as the counter electrode, and a saturated calomel electrode (SCE) as the reference electrode. An aqueous solution of 0.25 M K_2SO_3 and 0.35 M Na_2S (pH = 13.3) was used as the electrolyte, which was prepared using MILLIPORE water (resistivity 18.2 MΩ cm), degassing it by purging with high purity nitrogen, and then ultrasonicating for 30 min before each experiment. All the photoelectrochemical experiments were carried out under a stationary condition with nitrogen being bubbled through the electrolyte prior to and between all measurements, while it was kept flowing over the solution during the measurement. A copper wire was attached to the conducting layer of the working electrode with silver paste. The back and sidewall of the samples was covered with epoxy resin to prevent current leakage. The sample was then placed in the electrochemical cell at a distance of 5 cm from the quartz window. All the samples had an area of 1.0 cm^2. Current–voltage characteristics of the samples were obtained as a function of applied potential (−1.5 to +1.0 V *vs.* SCE) and under front-side illumination with a computer-controlled potentiostat (Autolab PGSTAT302). The scan rate was set at 2.5 mV s^{-1}. A 300 W Xe lamp (Perkin Elmer Model PE300UV) with UV-cut filter (>400 nm) was used as the light source. The light intensity was varied from 0 to 100 mW cm^{-2}. The intensity was measured by an optical power meter (Oriel Model 70310).

The electrochemical impedance spectroscopic (EIS) experiments were carried out with the same system mentioned in the previous paragraph. In the dark, the responses were recorded by sweeping the frequencies from 10 to 10^4 Hz at a certain applied voltage (from −1.1 to 0.0 V *vs.* SCE). A small sinusoidal signal of 10 mV was applied in addition to the bias potential. Under illumination, the light was shined on the semiconductor side of the working electrode. At the same time, the impedance measurements were carried out. The charge transfer parameters of the samples were retrieved by fitting the experimental data to the proposed models shown in Fig. 1.

Results and discussion

The basic idea of chemical bath deposition is the selective nucleation and growth on the substrate surfaces when the ion concentration products presented in the precursor solution exceed the solubility products. The mechanism of growth of binary metal sulfide thin films has been discussed thoroughly. Some reviews can be found.[24–27] Based on our experience, the quality of the Ag–In–S thin films, prepared by normal chemical bath deposition (CBD), depends strongly on the details of the experimental conditions, *e.g.*, humidity, chemical providers, temperature and *etc.* In fact, the vendor and purity of the indium nitrate is critical for repeatable results. Although good quality films can be fabricated by the CBD process, the yield is relatively low and very often the dark current density is high. We found that dense films are required to decrease the dark current density, *i.e.*, reduce the electron–hole charge recombination and the leakage current between the substrate and the electrolyte. In order to find a solution to mitigate aforementioned problems, we have to understand the mechanism of the CBD process. As stated in the literature, *e.g.* ref. 27 ion-by-ion deposition mechanism, or at least mixed ion-by-ion and cluster-by-cluster mechanism can increase the adhesion and interface properties. In such regards, ultrasonic vibration during chemical bath deposition offers a better way to make the film more homogeneous and compact.[13,14]

In addition, the operating window for the synthesis of stoichiometric $AgInS_2$ is rather small, as can be seen in the Ag_2S–In_2S_3 phase diagram.[28] The single phase $AgInS_2$ is generated only when the ratio of Ag/In is close to one. Not surprisingly, relatively more reports regarding the preparations and characterizations of $AgIn_5S_8$ thin films can be found in the literature.[21,22,29–31] In this study, however, we first reported the generation of homogeneous $AgInS_2$ thin films. Moreover, ultrasonic-assisted chemical bath deposition (UCBD) offers another wet process to generate thin films with the orthorhombic structure. Note that $AgInS_2$ thin films with the chalcopyrite phase, the low temperature stable phase, were usually reported using pyrolysis and electrodeposition.[10,32] Secondly, electrochemical impedance can be measured in the dark and under illumination. Therefore, the charge transfer mechanism can be interpreted for this visible light-active material.

Preparation of $AgInS_2$ photoanode

Based on our experience, metal ion concentrations have a profound influence.[11,15,23] Additionally, other parameters, such as reaction temperature, substrate surface properties, chelating agents, and *etc.*, must be tuned in order to obtain good quality thin films. In this study, $AgInS_2$ on ITO-coated glass substrates were generated when Ag/In was kept at 5. Fig. 2a shows the XRD patterns of the sample. Six major peaks at $2\theta = 24.992$, 25.427, 26.586, 28.382, 43.692, and 44.530° can be assigned to the (1 2 0), (2 0 0), (0 0 2), (1 2 1), (0 4 0), and (3 2 0) planes of orthorhombic $AgInS_2$ (o-$AgInS_2$, JCPDS 25-1328). Peaks at 30.580, 35.466, and 51.037° correspond to the diffraction from the ITO (JCPDS 06-0416) on top of the glass substrates. Fig. 2b shows the Raman spectrum of the prepared sample. Three crystal vibration peaks can be clearly seen between 200 and 400 cm^{-1}. The peaks at 275, 300, and 350 cm^{-1} can be assigned to o-$AgInS_2$.[33] Additionally, the spectrum shown in Fig. 2b can be distinguished from that of $AgIn_5S_8$. Hu *et al.* reported the synthesis of silver indium sulfide nanocrystals and indicated that a strong peak at 130 cm^{-1} can be assigned to $AgIn_5S_8$.[34] The absence of

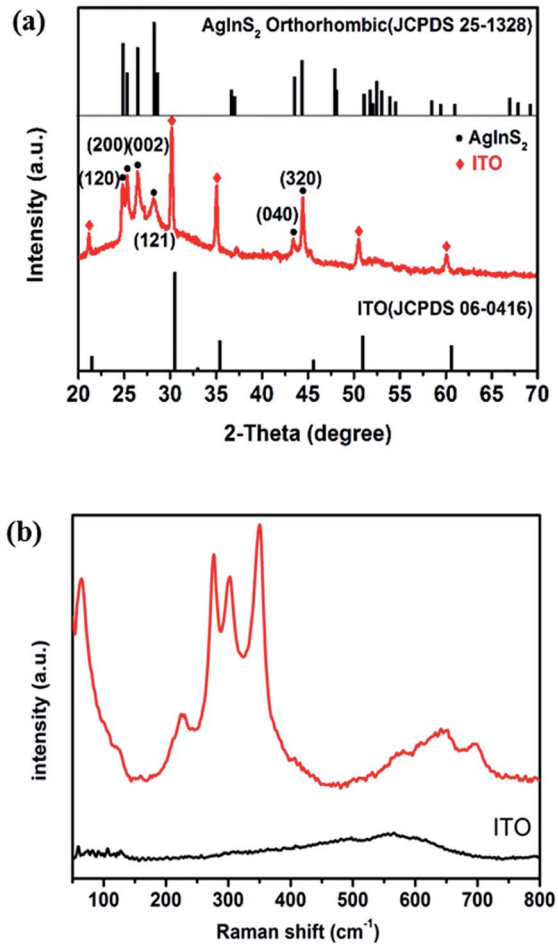

Fig. 2 (a) X-ray diffraction pattern of the $AgInS_2$ sample, and (b) Raman spectra of $AgInS_2$-coated and bare ITO-coated glass substrates.

the peak in our samples is evidence that $AgIn_5S_8$ is not present in our thin films. The Raman spectrum of bare ITO is also displayed for comparison. A broad peak at 550 cm^{-1} was observed, which agrees with the data reported.[35] The result suggests that the surface properties of the ITO-coated substrates and the solution chemistry used in our process favor the nucleation and growth of high temperature stable orthorhombic phase.

Fig. 3 exhibits the SEM images of the surface morphology and cross-section of the sample. The low-magnification SEM image, Fig. 3a, demonstrates that the $AgInS_2$ film covered the ITO-coated glass substrate uniformly. In addition, the high-magnification image, Fig. 3b, shows that a dense sheet-like structure was generated using the UCBD process. The microstructure is similar to that previously reported.[11,22] From Fig. 3c, the cross-sectional SEM image, the thickness was determined by averaging at least three different spots, and at least two images were used. The thickness of the sample is 758.9 ± 40.9 nm. Composition of the sample determined using EDS was Ag : In : S = 1 : 1.14 : 1.94, very close to the stoichiometric ratio of $AgInS_2$. Based on the crystal structures and compositional analyses, o-$AgInS_2$ films were obtained using the UCBD method.

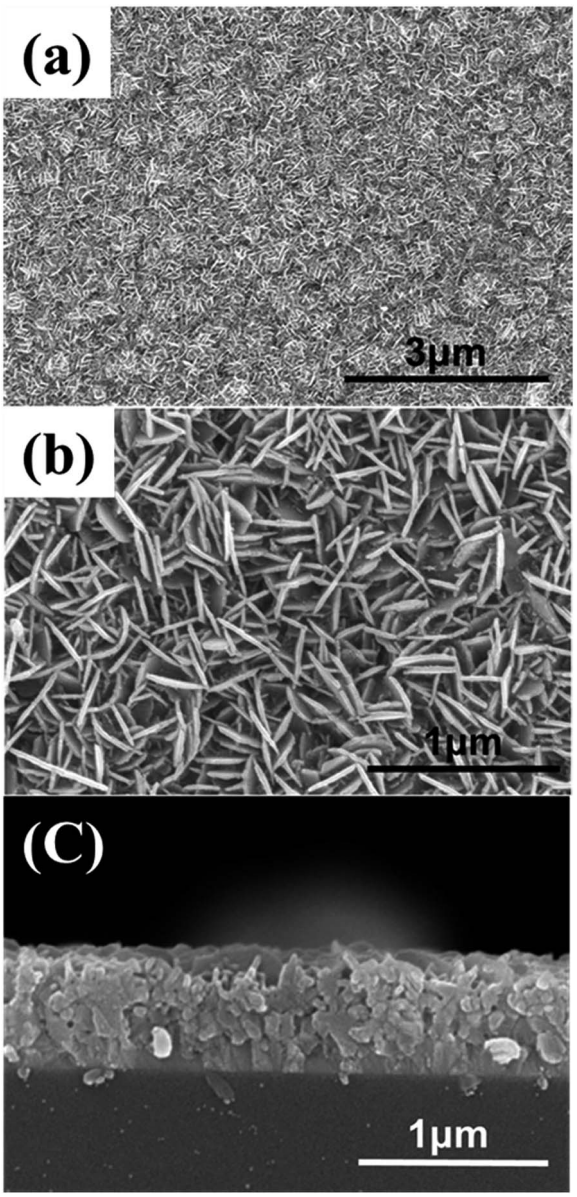

Fig. 3 SEM images of top-view (a) low magnification (15 K), (b) high magnification (100 K), and (c) cross-section of $AgInS_2$ film.

The optical properties were further characterized. Fig. 4 shows the transmittance and reflectance spectra recorded by UV-vis spectrometer with an integrating sphere. The transmission spectrum indicates that the sample exhibits a sharp absorption around 650 nm, with a relatively low reflectance (<6%). The optical band gaps can be estimated from the absorption spectra according to the following relationship:[36]

$$(\alpha h\nu) \propto (h\nu - E_g)^n \quad (1)$$

where $h\nu$ is the photon energy, E_g is the optical band gap, and α is the absorption coefficient which can be obtained from the following equation:

$$T(\lambda) = [1 - R(\lambda)]^2 \exp(-\alpha d) \quad (2)$$

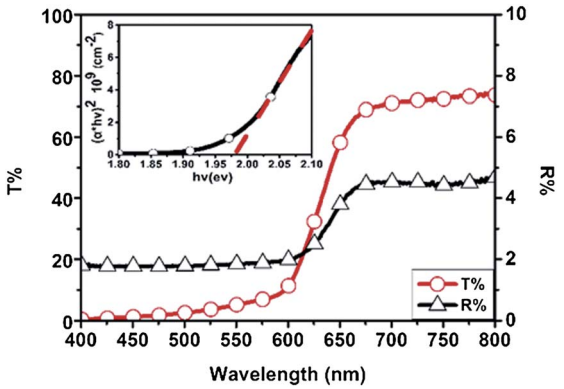

Fig. 4 Transmission and reflection spectra of the $AgInS_2$ film. Inset: $(\alpha h\nu)^2$ *vs.* $h\nu$ plot for energy gap determination. Open circle: transmittance; open triangle: reflectance.

where T is the transmission and R is the reflectance. n appeared in eqn (1) is 1/2 for direct band gap. The inset in Fig. 4 plots $(\alpha h\nu)^2$ against $h\nu$. The linear extrapolation to $(\alpha h\nu)^2 = 0$ gives the optical band gap. From this figure, the direct band gap of our sample is 1.98 eV. The value is in good agreement with that reported in the literature.[37]

Electrochemical impedance analysis

The electrochemical properties of the $AgInS_2$ thin film immersed in the sacrificial reagent (0.25 M K_2SO_3 and 0.35 M Na_2S) were scrutinized. This sacrificial reagent was used as the hole scavenger. SO_3^{2-} and S^{2-} ions as electron donors effectively suppress the photocorrosion of the metal sulfide photocatalyst.[38] Our photocurrent measurements indicated that the dark current of the sample (on the order of 10^{-7} A cm^{-2}) is much smaller than that of thinner samples ($\sim 10^{-4}$ A cm^{-2}). Considering the stability of the semiconductor thin films immersed in the electrolyte, the sample (thickness of 758.9 nm) was used exclusively for the electrochemical analysis. First, the open circuit potential (OCP) of this semiconductor–electrolyte interface in the dark and under intense illumination was measured, see Fig. 5. The thin film was placed vertically in the electrolyte overnight for equilibrium. The OCP in the dark decreased gradually and reached a stable potential of −0.73 V *vs.* SCE. This value should be the Fermi level of the electrolyte, and the decrease in OCP might be associated with the adsorption of the ions on the semiconductor surface. On the other hand, the OCP under intense illumination were rather stable, located at −0.84 V *vs.* SCE, corresponding to the flat band potential of the $AgInS_2$ photoanode. The flat band potential obtained using OCP method is relatively more positive than that obtained using other methods, *e.g.* Mott–Schottky method,[39] perhaps due to the charge recombination and slow charge-transfer kinetics at the semiconductor–electrolyte interface.

Fig. 6 shows the Nyquist plots of the impedance measurements from −0.1 to −0.6 V *vs.* SCE in the dark. A typical one semicircle was observed at all potentials. Randle's model, shown in Fig. 1c was used to retrieve the charge transfer resistance and space charge capacitance of the semiconductor. The flat band potential was determined by plotting $1/C^2$ as a function of applied potential and extrapolating the linear part to $1/C^2 = 0$, or so-called Mott–Schottky plot. From this figure, it follows that the flat band potential is approximately −1.1 V *vs.* SCE. The current potential measurements were carried out. Fig. 7 plots the photocurrent densities of the $AgInS_2$ sample in response to varying light intensities, from 9 to 75 mW cm^{-2}. From this figure, the photo-enhanced current density increases with light intensity. The anodic current started to rise at approximately −1.0 V, very close to the flat band potential determined using the Mott–Schottky plot. On the other hand, cathodic current appeared at approximately −1.2 V *vs.* SCE, both in the dark and under illumination.

The same electrochemical impedance analysis procedure can be applied to the semiconductor–electrolyte interface under illumination. Unlike the figures reported regarding the photoelectrochemical process,[17,20] only one semicircle was observed in our study (Fig. 8a). The Nyquist plot was obtained by sweeping the frequency in the range of 10 to 10^4 Hz. Three models were used to fit the impedance spectra under a 75 mW cm^{-2}-illumination at various applied voltages. However, the first two models, which take the surface states into consideration, cannot give reasonable parameters, *e.g.* negative

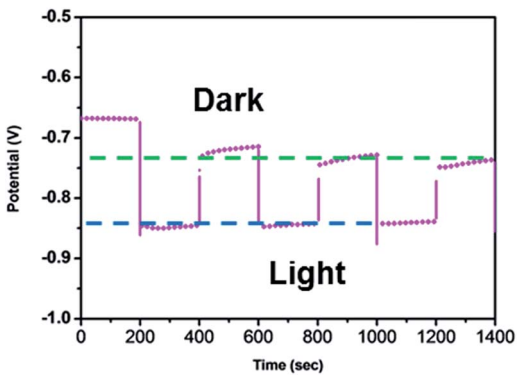

Fig. 5 Open circuit potential of the $AgInS_2$ electrode in the dark and under intense illumination.

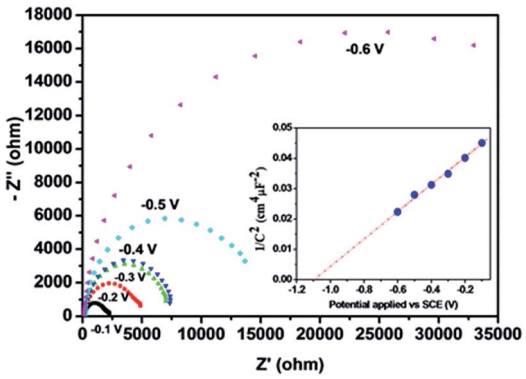

Fig. 6 Nyquist plot of sample at various applied potentials in the dark. Inset: Mott–Schottky plot determined in Na_2S and K_2SO_3 sacrificial reagent.

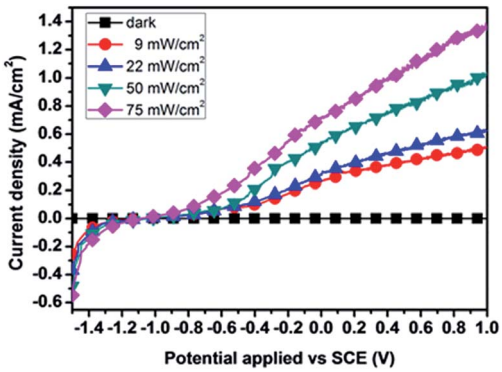

Fig. 7 Current densities of sample in response to various illumination intensities from 0 (dark), 9, 22, 50, and 75 mW cm^{-2}.

resistance ($R_{ct,trap}$) and zero exponent α in the constant phase element ($Z_{CPE} = Y_0(j\omega)^{-\alpha}$), appeared in Fig. 1b. The simplest model, Randle's circuit (Fig. 1c), however, was able to derive the fit parameters from the impedance spectra. More consistent results were obtained both in the whole frequency range (10 to 10^4 Hz) and high frequency range (10^3 to 10^4 Hz), as illustrated in Fig. 8b and c at the applied bias of −0.9 V *vs.* SCE, respectively.

The charge transfer resistance and space charge capacitance in the dark and under illumination were also plotted in Fig. 9a and b, respectively. The series resistance of the $AgInS_2$ film electrode in response to various bias voltages is in the range of 50 to 200 Ω, in agreement with the reported values. The charge transfer resistance in the dark is one order of magnitude larger than that under illumination. However, the resistance in the dark drops rather quickly starting from −0.6 V *vs.* SCE in the anodic direction, perhaps due to the Fermi level of the electrolyte and related to the oxidation kinetics from the valence band holes.[20] From this charge transfer resistance in the dark and the slope estimated from the Mott–Schottky plot (Fig. 6), it suggests that the $AgInS_2$ is relatively conductive, comparing to other photoanodes reported in the literature.[20,40] Note also that the charge transfer resistance under illumination peaks at −1.0 V *vs.* SCE, very close to the flat band potential determined previously (Fig. 6 inset). This value of peak voltage coincides with the onset of the photocurrent, shown in Fig. 7.

The space charge capacitances in the dark and under illumination are displayed in Fig. 9b. The values for C_{sc} show a distribution behavior under illumination, following similar trend as charge transfer resistance under illumination (Fig. 9a). The largest value of C_{sc} is located at −1.0 V *vs.* SCE, which is also very close to the flat band potential of $AgInS_2$ prepared in this study. However, the values of C_{sc} in the dark exhibit anomalous behavior at applied potential between −0.7 and −0.6 V *vs.* SCE. An order of magnitude difference in values of C_{sc} is observed. Note that this applied potential is in the vicinity of the Fermi level of the electrolyte, determined using OCP method (Fig. 5). When the applied voltage is more positive than the Fermi level of the electrolyte, the space charge region is further depleted. The electrolyte used in this study is a good electron donor. Fast

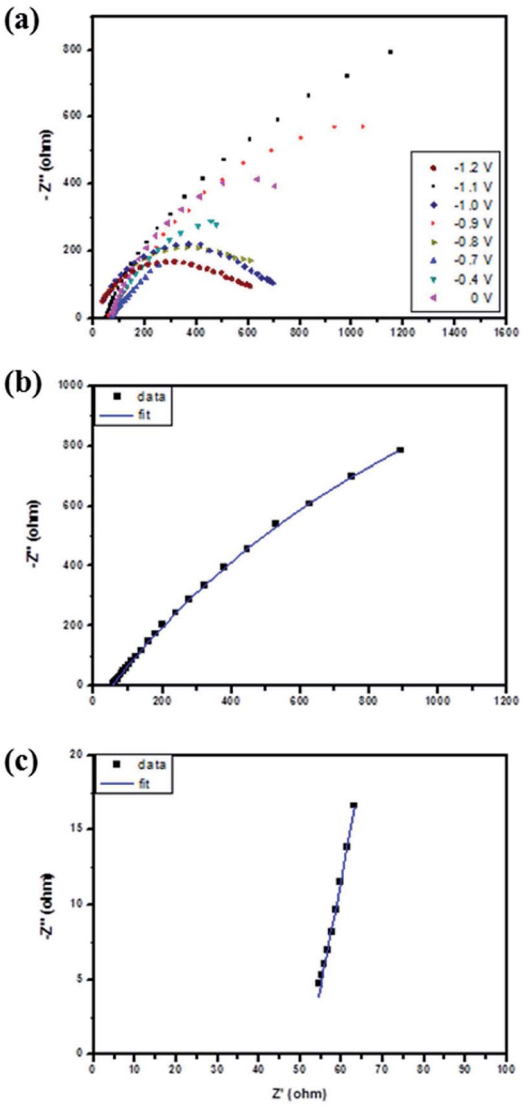

Fig. 8 Nyquist plot of the sample (a) at various applied potentials measured in the frequency range from 10 to 10^4 Hz. Detailed analysis of the sample at a bias of −0.9 V *vs.* SCE in the frequency range of (b) 10 to 10^4 Hz, and (c) 10^3 to 10^4 Hz. Square: data points. Solid line: fitted curve using Randle's model. All the measurements were carried out under illumination.

electron injection from the electrolyte to the semiconductor through the following reactions is possible:[38]

$$SO_3^{2-} + H_2O \rightarrow SO_4^{2-} + 2H^+ + 2e^- \quad (3)$$

$$2S^{2-} \rightarrow S_2^{2-} + 2e^- \quad (4)$$

$$S_2^{2-} + SO_3^{2-} \rightarrow S_2O_3^{2-} + S^{2-} \quad (5)$$

$$SO_3^{2-} + S^{2-} \rightarrow S_2O_3^{2-} + 2e^- \quad (6)$$

The absorption of anions and electron injections mentioned above, in the applied potential more positive than −0.6 V *vs.* SCE might be responsible for the increase in the values of C_{sc} observed in Fig. 9b. Nevertheless, the Mott–Schottky plot was

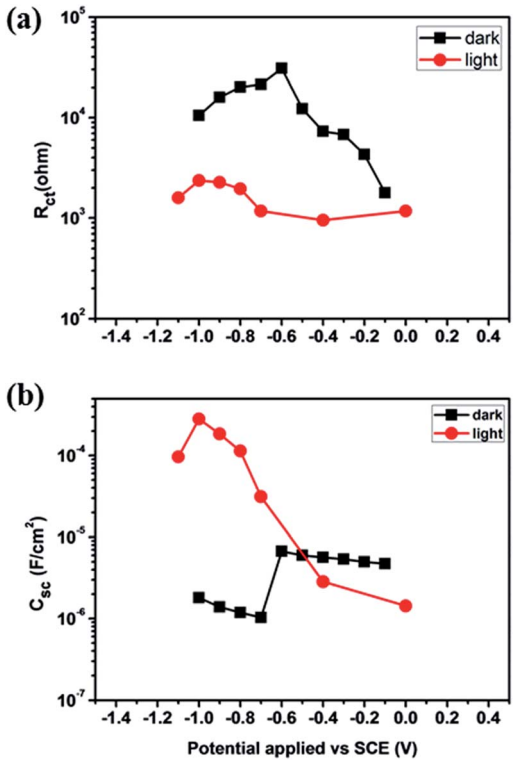

Fig. 9 (a) Charge transfer resistance and (b) space charge capacitance of the $AgInS_2$ photoanode retrieved from EIS analysis. Square: in the dark. Circle: under illumination.

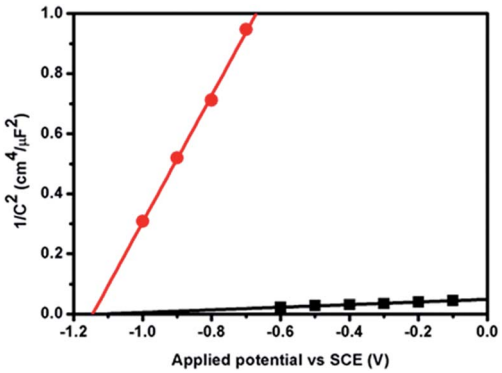

Fig. 10 Mott–Schottky plot of the $AgInS_2$ photoanode in contact with Na_2S and K_2SO_3 electrolyte in the dark. Circle: applied potential ranging from −1.0 to −0.7 V *vs.* SCE. Square: applied potential ranging from −0.6 to −0.1 V *vs.* SCE.

also generated from the bias potentials from −1.0 to −0.7 V *vs.* SCE. The flat-band potential obtained was located at −1.14 V (Fig. 10). However, the carrier density was lower, approximately 7.6 × 10^{18} cm^{-3}, comparing to ~10^{20} cm^{-3} determined from the linear region between −0.6 and −0.1 V *vs.* SCE. The carrier concentrations agree with the values reported in the literature.[41] Additionally, the positive slope from the Mott–Schottky plot indicates that the conduction of $AgInS_2$ prepared using UCBD is n-type.

The charge transfer resistance, space charge capacitance, and photocurrent density of the $AgInS_2$ photoanode under

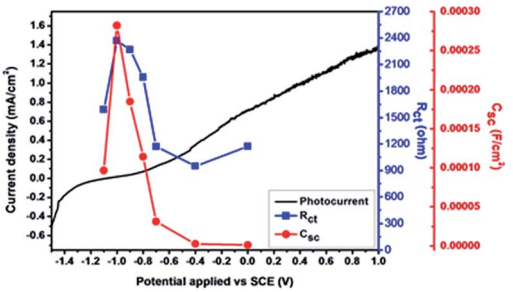

Fig. 11 Photo-enhanced current density, charge transfer resistance, and space charge capacitance of $AgInS_2$ photoanode under 75 mW cm^{-2} irradiation.

75 mW cm^{-2} illumination were plotted in Fig. 11. The charging of the semiconductor right before the onset of photocurrent was revealed, as well as an increase in charge transfer resistance. To this end, through a series of systematic investigations, the mechanism for minority-carrier (hole) transfer to the electrolyte from the valence band of the semiconductor photoanode directly was suggested to be the dominate pathway. This study has demonstrated that employing electrochemical impedance analysis, important parameters can be retrieved and the charge transfer mechanism can be elucidated.

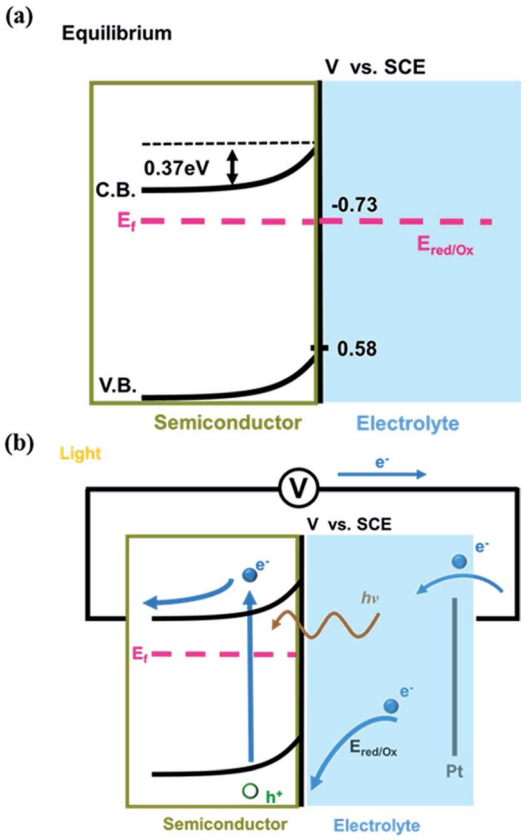

Scheme 1 Schematic diagram of the energy levels of $AgInS_2$ photoanode in the aqueous electrolyte (a) in the dark and (b) under illumination.

In summary, the relative energy levels of the conduction band and valence band of the $AgInS_2$ film, Fermi levels of the $AgInS_2$ film and the electrolyte are plotted in Scheme 1. In equilibrium (in the dark), the Fermi levels of the photoanode and electrolyte are aligned at −0.73 eV *vs.* SCE. The n-type characteristic of the $AgInS_2$ film causes the band bending and generates a depletion layer. Under light illumination, the $AgInS_2$ photoanode absorbs visible light with wavelengths shorter than approximately 650 nm, creating electron–hole pairs. Electrons transport to the counter electrode (Pt) due to the electric field within the depletion layer and external applied bias. The electrolyte, containing Na_2S and K_2SO_3, injects electrons into the semiconductor as the hole scavenger. The anodic photocurrent is then observed.

Conclusions

A $AgInS_2$ film was generated on an ITO-coated glass substrate using ultrasonic-assisted chemical bath deposition. The orthorhombic crystal structure was determined by employing XRD and Raman measurements. The photo-enhanced current density was observed in the visible light region. In addition, electrochemical impedance was employed to investigate the semiconductor–electrolyte interface, aiming to understand the charge transfer pathway of metal sulfides prepared in our laboratory. The peak position of space charge capacitance and charge transfer resistance strongly correlated to the onset of photocurrent, as illustrated in Fig. 11, strongly suggesting that the hole-transfer step takes place directly from the valence band. These findings may elucidate the mechanism of highly active Ag–In–S photoanodes.

Acknowledgements

The authors are grateful to the National Science Council of Taiwan and the Air Force Research Laboratory of USA for supporting this study. We thank the Instrument Center at National Central University and National Tsing-Hua University for SEM micrographs, XRD, and SIMS analysis. We also thank Professor Ya-Sen Sun's Lab at National Central University for UV-vis and Raman measurements.

Notes and references

1 B. Tell, J. L. Shay and H. M. Kasper, *J. Appl. Phys.*, 1972, **43**, 2469–2470.
2 S. M. Sze, in *Physics of Semiconductor Devices*, Jonh Wiley & Sons, New York, 2 edn, 1981, pp. 790–838.
3 W. Liu, D. B. Mitzi, M. Yuan, A. J. Kellock, S. J. Chey and O. Gunawan, *Chem. Mater.*, 2010, **22**, 1010–1014.
4 K. Derbyshire, in *Solid State Technology*, 2008.
5 G. Delgado, A. J. Mora, C. Pineda and T. Tinoco, *Mater. Res. Bull.*, 2001, **36**, 2507–2517.
6 S. Peng, S. Zhang, S. G. Mhaisalkar and S. Ramakrishna, *Phys. Chem. Chem. Phys.*, 2012, **14**, 8523–8529.
7 T. Sasamura, K.-i. Okazaki, A. Kudo, S. Kuwabata and T. Torimoto, *RSC Adv.*, 2012, **2**, 552–559.
8 P. Paul Ramesh, O. M. Hussain, S. Uthanna, B. Srinivasulu Naidu and P. Jayarama Reddy, *Mater. Lett.*, 1998, **34**, 217–221.
9 K.-W. Cheng, C.-M. Huang, G.-T. Pan, P.-C. Chen, T.-C. Lee and T. C. K. Yang, *Mater. Chem. Phys.*, 2008, **108**, 16–23.
10 C.-H. Wang, K.-W. Cheng and C.-J. Tseng, *Sol. Energy Mater. Sol. Cells*, 2011, **95**, 453–461.
11 W.-S. Chang, C.-C. Wu, M.-S. Jeng, K.-W. Cheng, C.-M. Huang and T.-C. Lee, *Mater. Chem. Phys.*, 2010, **120**, 307–312.
12 K.-W. Cheng, C.-M. Huang, G.-T. Pan, J.-C. Huang, T.-C. Lee and T. C. K. Yang, *J. Photochem. Photobiol., A*, 2009, **202**, 107–114.
13 Q. Liu and G. Mao, *Surf. Rev. Lett.*, 2009, **16**, 895–899.
14 A. Ichiboshi, M. Mongo, T. Akamine, T. Dobashi and T. Nakada, *Sol. Energy Mater. Sol. Cells*, 2006, **90**, 3130–3135.
15 C.-C. Wu, K.-W. Cheng, W.-S. Chang and T.-C. Lee, *J. Taiwan Inst. Chem. Eng.*, 2009, **40**, 180–187.
16 Z. Hens, *J. Phys. Chem. B*, 1998, **103**, 122–129.
17 P. Allongue and H. Cachet, *J. Electrochem. Soc.*, 1985, **132**, 45–52.
18 J. J. Kelly and R. Memming, *J. Electrochem. Soc.*, 1982, **129**, 730–738.
19 K. W. Frese, Jr and S. R. Morrison, *J. Electroanal. Chem.*, 1979, **126**, 1235–1241.
20 B. Klahr, S. Gimenez, F. Fabregat-Santiago, T. Hamann and J. Bisquert, *J. Am. Chem. Soc.*, 2012, **134**, 4294–4302.
21 C.-H. Lai, C.-Y. Chiang, P.-C. Lin, K.-Y. Yang, C. C. Hua and T.-C. Lee, *ACS Appl. Mater. Interfaces*, 2013, **5**, 3530–3540.
22 L.-H. Lin, C.-C. Wu, C.-H. Lai and T.-C. Lee, *Chem. Mater.*, 2008, **20**, 4475–4483.
23 L.-H. Lin, C.-C. Wu and T.-C. Lee, *Cryst. Growth Des.*, 2007, **7**, 2725–2732.
24 T. P. Niesen and M. R. De Guire, *Solid State Ionics*, 2002, **151**, 61–68.
25 R. S. Mane and C. D. Lokhande, *Mater. Chem. Phys.*, 2000, **65**, 1–31.
26 K. Yamaguchi, T. Yoshida, D. Lincot and H. Minoura, *J. Phys. Chem. B*, 2003, **107**, 387–397.
27 M. Froment and D. Lincot, *Electrochim. Acta*, 1995, **40**, 1293–1303.
28 V. P. Sachanyuk, G. P. Gorgut, V. V. Atuchin, I. D. Olekseyuk and O. V. Parasyuk, *J. Alloys Compd.*, 2008, **452**, 348–358.
29 A. F. Qasrawi, *Thin Solid Films*, 2008, **516**, 1116–1119.
30 L. Makhova, R. Szargan and I. Konovalov, *Thin Solid Films*, 2005, **472**, 157–163.
31 I. V. Bodnar and V. F. Gremenok, *Thin Solid Films*, 2005, **487**, 31–34.
32 Z. Aissa, T. B. Nasrallah, M. Amlouk, J. C. Bernede and S. Belgacem, *Sol. Energy Mater. Sol. Cells*, 2006, **90**, 1136–1146.
33 S. P. Hong, H. K. Park, J. H. Oh, H. Yang and Y. R. Do, *J. Mater. Chem.*, 2012, **22**, 18939–18949.
34 J. Q. Hu, B. Deng, K. B. Tang, C. R. Wang and Y. T. Qian, *J. Mater. Res.*, 2001, **16**, 3411–3415.
35 D. Pradhan, M. Kumar, Y. Ando and K. T. Leung, *ACS Appl. Mater. Interfaces*, 2009, **1**, 789–796.

36 J. Tauc, in *Amorphous and Liquid Semiconductors*, Plenum Press, London and New York, 1974, pp. 159–220.
37 J. L. Shay, B. Tell and L. M. Schiavone, *Phys. Rev. B: Solid State*, 1974, **9**, 1719–1723.
38 I. Tsuji, H. Kato, H. Kobayashi and A. Kudo, *J. Am. Chem. Soc.*, 2004, **126**, 13406–13413.
39 J. D. Beach, Jr, Ph.D., Colorado School of Mines, 2001.
40 Z. Hens and W. P. Gomes, *J. Phys. Chem. B*, 1998, **103**, 130–138.
41 K. Hattori, K. Akamatsu and N. Kamegashira, *J. Appl. Phys.*, 1992, **71**, 3414–3418.